Contents lists available at ScienceDirect

Arabian Journal of Chemistry

journal homepage: www.ksu.edu.sa

Chemical characterization of different parts of *Forsythia suspensa* and α-glucosidase and pancreatic lipase inhibitors screening based on UPLC-QTOF-MS/MS and plant metabolomics analysis

Yan-Li Ji [a,b,1], Xie Feng [a,b,1], Ya-Qing Chang [a,b], Yu-Guang Zheng [a,c], Fang-Jie Hou [a,b,*], Dan Zhang [a,b,*], Long Guo [a,b,*]

[a] *Traditional Chinese Medicine Processing Technology Innovation Center of Hebei Province, School of Pharmacy, Hebei University of Chinese Medicine, Shijiazhuang, China*
[b] *International Joint Research Center on Resource Utilization and Quality Evaluation of Traditional Chinese Medicine of Hebei Province, Hebei University of Chinese Medicine, Shijiazhuang, China*
[c] *Hebei Chemical and Pharmaceutical College, Shijiazhuang, China*

ARTICLE INFO

Keywords:
Forsythia suspensa
UPLC-QTOF-MS/MS
Plant metabolomics analysis
α-Glucosidase
Pancreatic lipase
Molecular docking analysis

ABSTRACT

Forsythia suspensa (Thunb.) Vahl (FS) is an important plant with high edible and medicinal values. The edible fruit of FS is a common traditional medicine in China, Japan and Korea. Compared to the research on the phytochemistry and pharmacology of the fruits, study on the other parts of FS, such as leaves and flowers is still limited. In this study, an integrated strategy based on ultra-performance liquid chromatography quadrupole time of flight mass spectrometry (UPLC-QTOF-MS/MS), plant metabolomics and correlation analysis was established for comprehensively chemical characterization of fruits, leaves and flowers of FS, and discovery of α-glucosidase and pancreatic lipase inhibitory metabolites. The plant metabolic profiling of fruits, leaves and flowers of FS was performed by UPLC-QTOF-MS/MS, and a total of 74 secondary metabolites, including 15 phenylethanoid glycosides, 20 lignans, 10 cyclohexanol derivatives, 11 organic acids, 9 flavonoids, 3 triterpenes, and 10 other compounds were identified. Then, 29 differential secondary metabolites that responsible to distinguish the fruits, leaves and flowers of FS were further screened out by multivariate statistical analysis. Meanwhile, the α-glucosidase and pancreatic lipase inhibition of different parts of FS were evaluated and compared by *in vitro* experiments. The results demonstrated that the leaves of FS showed the highest inhibition on α-glucosidase and pancreatic lipase with IC_{50} of 0.17 ± 0.04 mg/mL and 0.56 ± 0.33 mg/mL, respectively. Then, the correlation between differential metabolites and enzyme inhibitory activities were investigated by Pearson correlation analysis, and 12 potential α-glucosidase and pancreatic lipase inhibitors were screen out. Additionally, the α-glucosidase and pancreatic lipase inhibitory activities of five potential enzyme inhibitory components, including quercitrin, rutin, kaempferol-3-O-rutinoside, pinoresinol-4-O-glucoside and phillyrin were further validated by *in vitro* assays and molecular docking analysis. The results showed that all the five potential inhibitors showed good inhibitory effects on α-glucosidase and pancreatic lipase, and the binding of the five inhibitors to enzymes mainly through hydrogen bonding, hydrophobic force, and ionic bonding. This study provided a feasible strategy for comparison and discrimination of different parts of medicinal plant and discovery of bioactive components, and also provided useful information for future utilization of different parts of FS.

1. Introduction

Forsythia suspensa (Thunb.) Vahl. (FS) is a shrub belonging to Oleaceae, which is mainly distributed in East Asia, such as China, Japan, and Korea. As an important medical herb, FS has high edible and medicinal values (Wang et al., 2018). The fruit of FS (Forsythia Fructus) is a

* Corresponding authors at: Traditional Chinese Medicine Processing Technology Innovation Center of Hebei Province, School of Pharmacy, Hebei University of Chinese Medicine, Shijiazhuang, China.
E-mail addresses: 15130687505@163.com (F.-J. Hou), zhangdanid@163.com (D. Zhang), guo_long11@163.com (L. Guo).
[1] These two authors contributed equally to this work.

https://doi.org/10.1016/j.arabjc.2024.105723
Received 17 September 2023; Accepted 10 March 2024
Available online 12 March 2024

commonly used traditional medicine with the efficacy to treat pyrexia, inflammation, gonorrhea, carbuncle and erysipelas (Chinese Pharmacopoeia Commission, 2020). Modern pharmacological researches found that FS has multiple pharmacological activities, such as anti-inflammatory, antioxidant, anti-virus, antibacterial, anti-liver injury, anti-diabetes and anti-hyperlipidemia (Shao et al., 2021; Zhang et al., 2016). Phytochemical studies showed that the fruits of FS contained a large amount of bioactive secondary metabolites, including lignans, phenylethanoid, flavonoids, phenolic acids and triterpenoids (Kuo et al., 2017).

The biological activities of different plant tissues of the same species varied greatly due to the difference of bioactive metabolites accumulation (Kandida et al., 2023). Up to now, most of the studies focused on chemical characterization and pharmacological activities of the fruit of FS due to its medicinal values (Pan et al., 2022). The leaves and flowers of FS are widely consumed as tea in Asian areas, but research on their chemical compositions and bioactivities are still limited. Several studies about the leaves and flowers of FS have been carried out, which revealed that the chemical compositions of leaves and flowers were similar to those of fruits (Ge et al., 2016; Zhou et al.,2022). However, there has been no comprehensive study and discussion on chemical comparison of different parts (fruits, leaves and flowers) of FS. It is reported that the leaves of FS possessed great α-glucosidase and pancreatic lipase inhibition effects (Chen et al., 2017). Whether fruits and flowers of FS also have α-glucosidase and pancreatic lipase inhibitory activities are still unknown, and the investigation of α-glucosidase and pancreatic lipase inhibitory components of different parts of FS is also lack of study. Thus, it is necessary to characterize and compare the chemical profiles of fruits, leaves and flowers of FS, and discover the α-glucosidase and pancreatic lipase inhibitors in FS.

Metabolomics is an important part of systems biology, which can characterize metabolites with low molecular weight in biological system, such as plasma, urine, cells, and tissues (Wörheide et al., 2021). Metabolomics techniques could observe abnormal changes of endogenous metabolites before the appearance of physiological or pathological damages, and reflect the function of organisms from terminal symptoms of metabolic network (Li et al., 2020). Plant metabolomics is an important branch of metabolomics, which has been widely used for discovery of new natural product-based drugs, quality control of herbal medicines, and pharmaceutical production for the benefit of human health (Scossa et al., 2018; Kurniawan et al., 2023). Plant metabolomics is also commonly used to compare metabolic profiles among different samples, and identify differences associated with the underlying study question (Zhang et al., 2021; Yang et al.,2022). In plant metabolomics, gas chromatography-mass spectrometry (GC–MS), liquid chromatography-mass spectrometry (LC-MS), and proton nuclear magnetic resonance spectroscopy (1H NMR) are commonly used analysis techniques (Jia et al., 2015; Cui et al., 2018). LC-MS possesses the advantages of wide analysis range, strong separation ability, fast analysis time, and suitable for most metabolite detection and analysis, which is the most widely used technique in plant metabolomics (Tsugawa et al., 2021). LC-MS based plant metabolomics not only can maximize the information of metabolites in plant tissues, but also help to clarify the overall metabolite group profile of the measured substances, which is an ideal method to comprehensively characterize the secondary metabolites and explore the differential metabolites in different parts (fruits, leaves and flowers) of FS (Li et al., 2021; Salem et al., 2023).

In this present work, an integrated strategy based on ultra-performance liquid chromatography quadrupole time of flight mass spectrometry (UPLC-QTOF-MS/MS), plant metabolomics and correlation analysis was developed for comparison of secondary metabolites of fruits, leaves and flowers of FS, and discovery of α-glucosidase and pancreatic lipase inhibitors.. The flowchart of the integrated strategy is shown in Fig. 1. Firstly, an UPLC-QTOF-MS/MS was employed to characterize the secondary metabolites of different parts of FS samples. Then, the plant metabolomics analysis was performed based on the plant metabolic profiles of fruits, leaves and flowers of FS. Principal component analysis (PCA) and orthogonal partial least squares discriminant analysis (OPLS-DA) were used to compare the metabolic profiles of FS fruits, leaves and flowers and find the differential metabolites. Meanwhile, the inhibitory activities of different part of FS samples on α-glucosidase and pancreatic lipase were evaluated by *in vitro* inhibition assay. Pearson correlation analysis was further employed to explore the correlation between characteristic metabolites and enzyme inhibitory activities of FS, and screen out potential enzyme inhibitors. Additionally, the α-glucosidase and pancreatic lipase inhibitory capacities of several selected compounds were validated, and the underlying inhibition mechanisms on enzymes were preliminarily investigated by

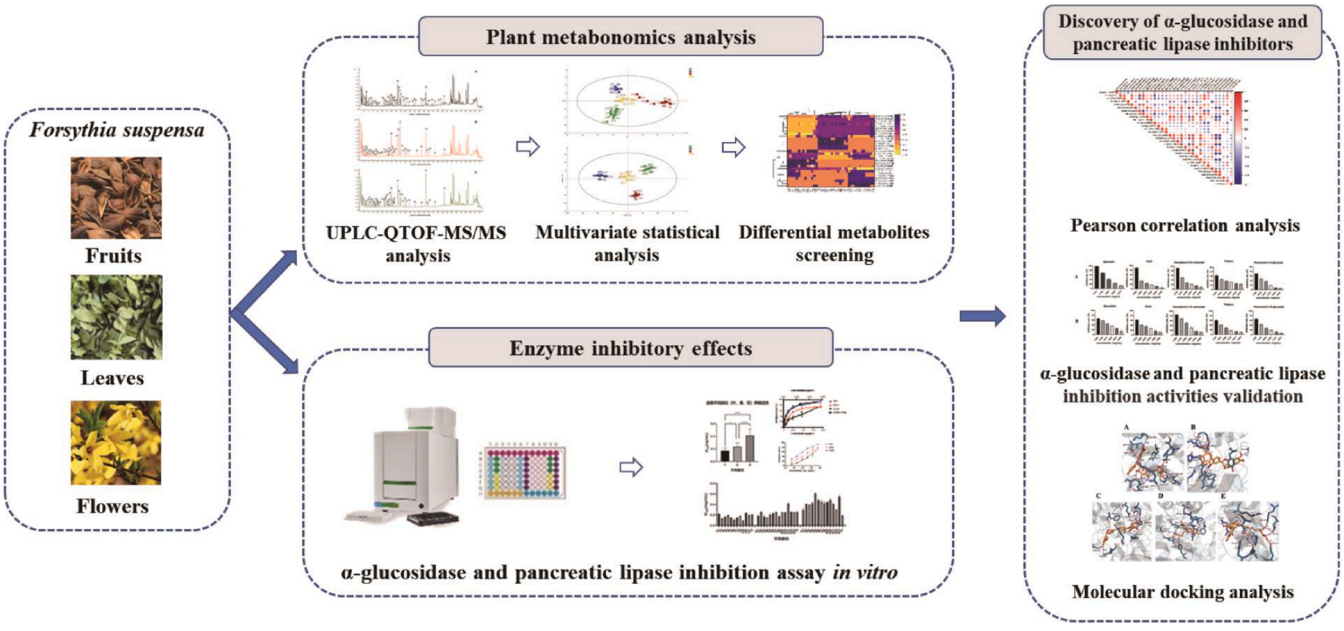

Fig. 1. The flowchart of the integrated strategy for comparison of secondary metabolites and discovery of α-glucosidase and pancreatic lipase inhibitors in different parts of *Forsythia suspensa*.

molecular docking analysis.

2. Material and methods

2.1. Plant material

14 batches of fruits of FS (G1-G14), 14 batches of flowers of FS (H1-H14) and 12 batches of leaves of FS (Y1-Y12) were collected in Hebei, Shanxi, and Henan provinces in northern China, and all the batches of different parts of FS samples were dried in the shade and stored in desiccator. The voucher specimens that identified by Associate Professor Guo Long have been deposited at Hebei Provincial Technology Innovation Center of Chinese Medicine Processing, Hebei University of Chinese Medicine. Sample information of different parts of FS are shown in Supplementary Table S1.

2.2. Instruments

The chemical characterization of different parts of FS were performed on Agilent 1290–6545 UPLC-QTOF-MS/MS system (Agilent Technologies, Santa Clara, USA). Chromatographic separation was performed on ACQUITY UPLC BEH C18 column (Waters, Milford, USA). The absorbance in α-glucosidase and pancreatic lipase inhibitory activities was measure by VICTOR Nivo multimode microplate reader (PerkinElmer, Waltham, USA). Ultrapure water was prepared by a Synergy water purification system (Millipore, Billerica, United States).

2.3. Materials and reagents

The reference standards of isochlorogenic acid B, rutin, quercetin, kaempferol-3-O-rutinoside, pinoresinol-4-O-glucoside, phillyrin, phillygenin were purchased from Chengdu Must Bio-Technoligy Co., Ltd. (Chengdu, China). α-Glucosidase, p-nitrophenyl-α-D-glucopyranoside (p-NPG), porcine pancreatic lipase (type II), 4-methylumbelliferyl oleate (4-MUO) were purchased from Sigma-Aldrich (St Louis, MO, United States). HPLC grade methanol, acetonitrile and formic acid were obtained from Fisher Scientific (Pittsburgh, PA, United States). Other chemicals and reagents were of analytical grade.

2.4. Extraction procedure

The samples of fruits, flowers and leaves of FS were crushed and passed through 40 mesh sieves. 0.1 g of sample powder was accurately weighed and mixed with 7 mL of 70 % (v/v) methanol, sonicated for 1 h, and adjusted to the initial weight by adding 70 % methanol (v/v) as needed. The sample was centrifuged at 13000 rpm/min for 10 min, 200 μL of the supernatant was removed and diluted 10 times, and 50 μL of isochlorogenic acid B solution (1.2 mg/mL) was added precisely as internal standard. Then, the supernatant was filtered through a 0.22 μm membrane before UPLC-QTOF-MS/MS analysis. For α-glucosidase and pancreatic lipase inhibition experiments, 600 μL of the above-extracted sample of different parts of *Forsythia suspensa* was taken out, the solvent was evaporated to remove the organic solvents and re-dissolved with equal volumes of phosphate buffer and Tris-HCl buffer, respectively.

2.5. Chemical profile of different parts of Forsythia suspensa by UPLC-QTOF-MS/MS

The UPLC-QTOF-MS/MS analysis of fruits, flowers and leaves of FS was carried out on an Agilent 1290 infinity UPLC system coupled with an Agilent 6545 quadrupole time-of-flight mass spectrometer system (Agilent Technologies, Santa Clara, USA). Chromatographic separation was performed on an ACQUITY UPLC BEH C18 column (2.1 mm × 100 mm, 1.7 μm, Waters, Milford, USA). The mobile phases were consisted of 0.1 % formic acid water (A) with methanol (B) at a flow rate of 0.3 mL/min. The linear gradient elution was optimized as follows: 0–5 min, 10 % B; 5–15 min, 10–15 % B; 15–20 min, 15 % B; 20–26 min, 15–20 % B; 26–32 min, 20–25 % B; 32—40 min, 25–50 % B. The column temperature was maintained at 30 °C, and the injection volume was 1 μL. The MS parameters were set as follows: drying gas (N_2) temperature, 320 °C; drying gas (N_2) flow rate, 10.0 L/min; sheath gas temperature, 350 °C; sheath gas flow (N_2) rate, 11 L/min; nebulizer gas pressure, 35 psi; fragmentor voltage, 135 V; capillary voltage, +4000 V; collision energy, 40 eV. Data acquisition was performed on Agilent MassHunter Workstation (Agilent Technologies, Santa Clara, CA, USA). In addition, the quality control (QC) samples were prepared by mixing equal volumes of each test solution and used to assess system stability and data reproducibility. The QC samples were alternated every 5 injections, and analyzed in a data-dependent MS tandem.

2.6. Metabolomic analysis

Peak filtering, matching, calibration and normalization of metabolomics data were performed on Agilent Mass Profiler Professional B.06 software (Agilent Technologies, Santa Clara, CA, USA). Compound abundance was log 2 transformed, and normalized by the parent nuclear ion ($[M + H]^+$ 517.1633) of the internal standard (isochlorogenic acid B). Then, the metabolomic data was exported into SIMCA 14.1 (Umetrics, Malmo, Sweden) for PCA and OPLS-DA.

2.7. α-Glucosidase and pancreatic lipase inhibitory activities in vitro

To measure the α-glucosidase inhibition of different parts of FS, the experimental method was slightly adapted from literature (Chang et al., 2022). Briefly, 20 μL of FS samples were mixed with 75 μL of phosphate buffer (0.1 M, pH 6.9) and 65 μL of α-glucosidase solution (1 U/mL) in a 96-well plate. Pre-incubation for 15 min at 37℃, then the reaction was started by addition of 30 μL of p-NPG (2 mM). After incubation for 20 min at 37 ℃, the reaction was stopped by adding 50 μL of Na_2CO_3 (0.2 M). The absorbance (A_{sample}) was measure by a microplate reader at 405 nm. The background sample ($A_{background}$) was prepared by replacing the α-glucosidase solution with the same volume of phosphate buffer. The control sample ($A_{control}$) was using phosphate buffer instead of FS sample solution. The blank sample (A_{blank}) was prepared by adding phosphate buffer instead of α-glucosidase solution and FS sample solution. All the samples were analyzed in triplicate with five different concentrations, and the α-glucosidase inhibition (%) was calculated as follows:

α-glucosidase inhibition (%) = 1 - (A_{sample} − $A_{background}$)/($A_{control}$ − A_{blank}) × 100.

The inhibitions of different parts of FS on pancreatic lipase were assessed according to literatures (Chang et al., 2021). The FS samples, pancreatic lipase, and 4-MUO were prepared in Tris-HCl buffer solution (pH 8.0). 25 μL of FS samples and 25 μL of pancreatic lipase solution (1 mg/mL) were added into a black bottom 96-well plate. Pre-incubation for 10 min at 37 °C, the reaction was started by addition of 50 μL of 4-MUO solution (1 mM). After incubation for 20 min at 37℃, the reaction was stopped by adding 100 μL of 0.1 M citrate buffer solution (PH 4.2). The amount of 4-methylumbelliferone released by the pancreatic lipase was measured with a fluorometric microplate reader with an excitation wavelength at 355 nm and an emission wavelength at 460 nm. The background sample ($A_{background}$) was prepared by replacing the pancreatic lipase solution with the same volume of buffer solution. The control sample ($A_{control}$) was prepared by adding buffer solution instead of the FS sample. The blank sample (A_{blank}) was prepared by adding buffer solution instead of pancreatic lipase solution and FS sample solution. All the samples were analyzed in triplicate with five different concentrations, and the pancreatic lipase inhibition (%) was calculated as follows:

$$pancreaticlipaseinhibition(\%) = 1 - \left(A_{sample} - A_{background}\right)/\left(A_{control} - A_{blank}\right) \times 100$$

The α-glucosidase and pancreatic lipase inhibitory activities of different parts of FS samples were expressed as the concentration of sample with 50 % reduction in enzyme activity (IC_{50}), which was obtained by non-linear regression analysis of α-glucosidase and pancreatic lipase inhibition (%) versus sample concentration (mg/mL extracts equivalents) curves using GraphPad Prism version 9.0 (GraphPad Software, San Diego, CA, USA).

The α-glucosidase and pancreatic lipase inhibitory activities of selected potential α-glucosidase and pancreatic lipase inhibitors (rutin, quercetin, kaempferol-3-O-rutinoside, pinoresinol-4-O-glucoside, phillyrin) were determined and the IC_{50} values were also calculated.

2.8. Pearson correlation analysis

Pearson correlation analysis was employed to explore the correlation between the characteristic metabolites and α-glucosidase and pancreatic lipase inhibitory activities of fruits, flowers and leaves of FS. Taking the Pearson correlation coefficient as an index, the abundance of the characteristic metabolites in different parts of FS samples was set as one set of independent variables, and α-glucosidase or pancreatic lipase inhibitory activities (IC_{50} values) was set as the other set of independent variables. Then, Pearson correlation coefficients between the characteristic metabolites and IC_{50} values were calculated by SPSS 22.0 statistics software (SPSS Inc., Chicago, IL, United States).

2.9. Molecular docking analysis

To provide deep insight into the interaction effects between the screened inhibitors and enzymes, the molecular docking analysis was carried out based on the method described in previous literatures (Darwish et al., 2022). The crystal structures of α-glucosidase (PDB ID: 3A4A) and pancreatic lipase (PDB ID: 1LPB) were obtained from the RCSB Protein Data Bank (https://www.rcsb.org). The receptors were imported into Maestro 13.1 and preprocessed by Protein Preparation Wizard in the Schrodinger software to remove unnecessary water molecules, followed by hydrogen bond network optimization. The LigPrep module in the Schrodinger software was used to process ligands to generate possible three-dimensional (3D) structures. The Glide Grid Generation Wizard was used to generate docking grids. The docking grids was set as a 20 Å × 20 Å× 20 Å square pocket. The enzyme activity site coordinates between the ligand and 1LPB receptor protein was X: 11.12, Y: 20.24, Z: 48.25. The enzyme activity site coordinates with 3A4A receptor protein was X: 13.5, Y: −10.3, Z: 17.57. Molecular docking was performed under the Ligand Docking wizard, using SP and XP modes. The docking number output was set to 10, and the number of ligands docking energy optimization cycles was set to 100. Using MM-GBSA technology provided by Glide module and Prime module, the ligand binding energies and ligand strain energies could be calculated for each small molecule ligand and two proteins (1LPB and 3A4A), and the contribution value of hydrogen bond and the stability of binding could be shown. The final result was based on XP Gscore as the evaluation criterion. PYMOL was further used for visual analysis of possible binding interactions between inhibitors and enzymes.

3. Results and discussion

3.1. Chemical profile of different parts of Forsythia suspensa by UPLC-QTOF-MS/MS

For the comprehensive characterization of secondary metabolites in different parts of FS, the crude extracts of fruits, flowers and leaves of FS were analyzed by UPLC-QTOF-MS/MS. To achieve a maximum sensitivity for secondary metabolites, the effects of the ionisation parameters including ionisation mode, nebulizer gas pressure, electrospray voltage of the ion source and collision energy were investigated. The detection signal in positive ion mode was better than that in negative ion mode because of sensitivity and selectivity. Under the optimized chromatographic condition, most of the secondary metabolites in different parts of FS were well separated, and the typical total ion chromatograms of fruits, flowers and leaves of FS are displayed in Fig. 2. Combining the retention time, mass-to-charge ratio, fragmentation patterns, previous literatures and databases, the secondary metabolites were identified (Chen et al., 2017; Zhang et al., 2020; Li et al.,2022; Zhou et al.,2022). A total of 74 secondary metabolites, including 15 phenylethanoid glycosides, 20 lignans, 10 cyclohexanol derivatives, 11 organic acids, 9 flavonoids, 3 triterpenes, and 10 other constituents were identified or tentatively identified in three different parts of FS. The identification information, such as retention time, molecular formula, molecular ions and MS/MS fragments is summarized in Table 1, and the chemical structures of the 74 secondary metabolites are shown in Supplementary Fig. S1.

Phenylethanoid glycosides are one of the main bioactive compounds in FS. Forsythoside A was taken as an example to explore the fragmentation patterns of phenylethanoid glycosides. In the MS/MS spectrum (Supplementary Fig. S2), forsythoside A produced a protonated ion $[M + H]^+$ at *m/z* 625.1893. Due to the loss of caffeoyl and H_2O, forsythoside A exhibited fragment ions at *m/z* 463.1652 $[M + H\text{-}C_9H_6O_3]^+$ and 445.1489 $[M + H\text{-}C_9H_6O_3\text{-}H_2O]^+$. Caffeic acid-related fragment ions, such as *m/z* 181.0481 $[C_9H_8O_4 + H]^+$, 163.0325 $[C_9H_8O_4 + H\text{-}H_2O]^+$, and 137.0566 $[C_9H_8O_4 + H\text{-}CO_2]^+$ were also observed in the MS/MS spectra of phenylethanoid glycosides. According to the characteristic fragmentation patterns of phenylethanoid glycosides, a total of 15 phenylethanoid glycosides, including hydroxytyrosol glucoside (8), forsythoside E (14), R-suspensaside A (31), S-suspensaside A (32), calceolarioside A (34), calceolarioside C (36), forsythoside I (40), lianqiaoxinoside C (43), forsythoside H (47), forsythoside B (48), forsythoside A (49), calceolarioside B (51), suspensaside A (55), acteoside (57) and forsythenside K (61) were identified in different parts of FS.

Lignans are also one of the major active constituents of FS. The MS/MS fragmentation behavior of lignans was investigated using phillyrin. As shown in Supplementary Fig. S3, phillyrin showed a strong protonated ion $[M + Na]^+$ at *m/z* 557.1974 with the molecular formula $C_{27}H_{34}O_{11}$. The main fragment ions of phillyrin appeared at *m/z* 395.1477 $[M + Na\text{-}C_6H_{10}O_5]^+$ and *m/z* 380.1183$[M + Na\text{-}C_6H_{10}O_5\text{-}CH_3]^+$, which were due to the loss of the glucose ($C_6H_{10}O_5$) and CH_3. A total of 20 lignans including 8-hydroxypinoresinol-4-glucoside (28), isolariciresinol-4-O-glucoside (35), 8-hydroxypinoresinol-4′-glucoside (37), lariciresinol-9-O-glucoside (42), pinoresinol-4-O-glucoside (54), epi-pinoresinol-4-O-glucoside (56), epi-pinoresinol-4′-O-glucoside (58), agastinol (59), demethylphillyrin (60), (+)-pinoresinol monomethyl ether-β-D-glucoside (63), suspenoidside B (64), matairesinoside (65), phillyrin (66), arctiin (67), arctigenin (68), (+)-pinoresinol (69), (-)-pinoresinol (71), epipinoresinol (72), matairesinol (73) and phillygenin (74) were identified from the different parts of FS samples.

Forsythenside B is a typical cyclohexanol derivative in FS. Forsythenside B exhibited the protonated ion $[M + Na]^+$ at *m/z* 489.1355 ($C_{22}H_{26}O_{11}$). Its fragment ions were at *m/z* 339.1818 $[M + Na\text{-}C_8H_6O_3]^+$, 321.0945 $[M + Na\text{-}C_8H_6O_3\text{-}H_2O]^+$, 177.0521 $[M + Na\text{-}C_8H_6O_3\text{-}C_6H_{10}O_5]^+$ and 159.0521 $[M + Na\text{-}C_8H_6O_3\text{-}H_2O\text{-}C_6H_{10}O_5]^+$, which were typically characterized by the loss of sugar moieties and H_2O (Supplementary Fig. S4). Thus, 10 cyclohexanol derivatives such as rengynic acid-4-O-β-D-glucoside (1), galiridoside (7), 6′-methoxypolygoacetophenoside (9), vanilloloside (12), salidroside (13), forsythenside B (16), rengyoside D (26), rengyoside C (27), forsythenside A (30) and forsythenside H (52) were characterized in different parts of FS.

Organic acids contained in FS are mainly caffeoylquinic acids or its derivatives. Caffeoylquinic acids can present distinct fragments of caffeic acid and quinic acid, such as *m/z* 181 and 193 in positive ion mode. For example, chlorogenic acid showed the precursor ion $[M + H]^+$ at *m/z* 355.1022 ($C_{16}H_{18}O_9$), and the fragment ions at *m/z* 181.0342 [caffeoyl + H]$^+$, 163.0386 $[M + H\text{-}C_9H_6O_3\text{-}H_2O]^+$, and 145.0283 [M + H-

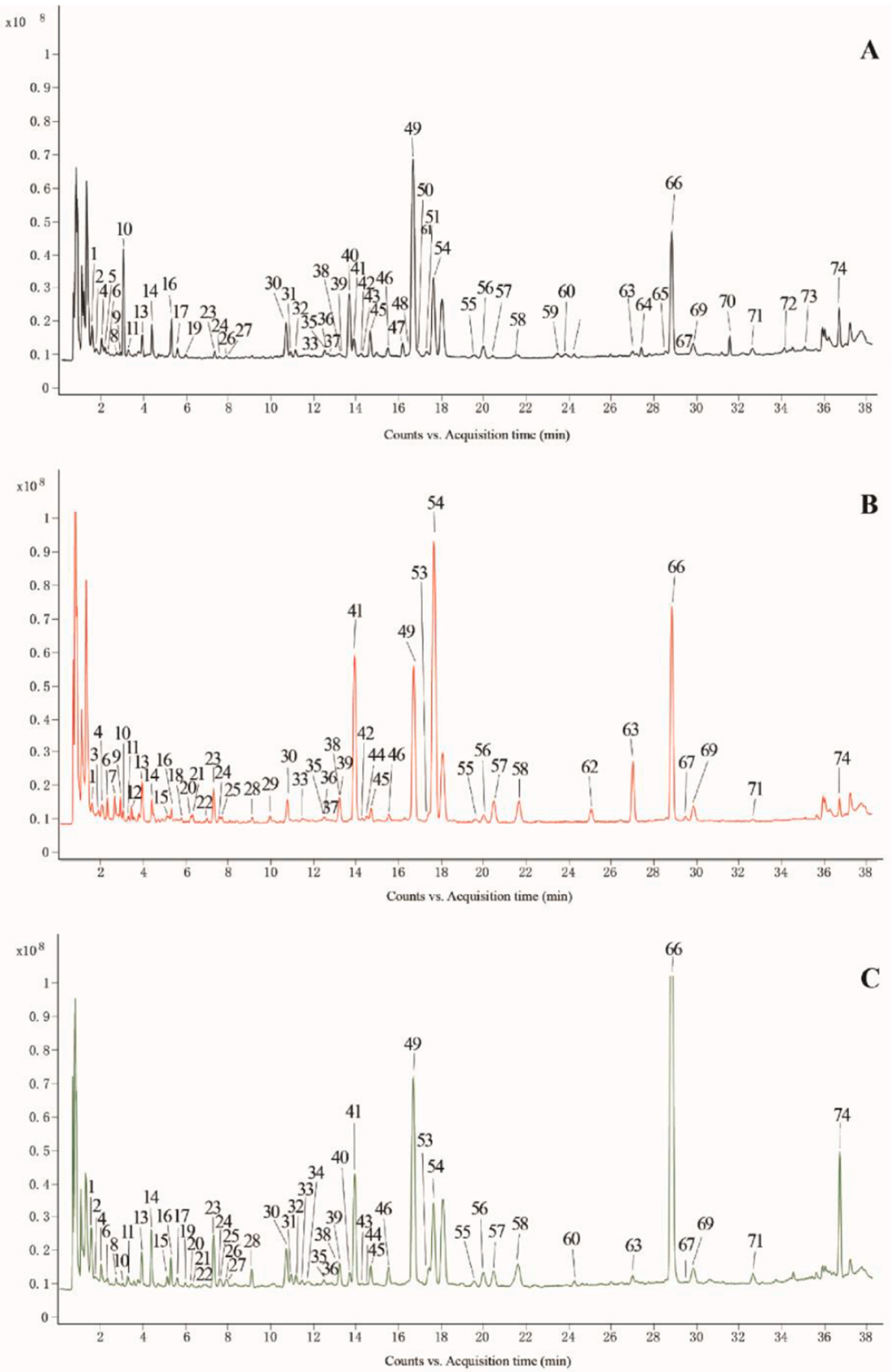

Fig. 2. The typical total ion chromatograms of fruits (A), flowers (B) and leaves (C) of *Forsythia suspensa* by UPLC-QTOF-MS/MS. The peak numbers are consistent with the compound numbers presented in Table 1.

Table 1
Information of 74 secondary metabolites in three parts of *Forsythia suspensa* identified by UPLC-QTOF-MS/MS.

No.	t_R (min)	Compounds	Molecular formula	Molecular ions (*m/z*) (mass accuracy)	Diff (ppm)	MS/MS fragments (*m/z*)	Classification	Fruits	Flowers	Leaves	References
1	1.586	Rengynic acid-4-O -β-D-glucoside	$C_{14}H_{24}O_9$	$[M+Na]^+$ 359.1311	0.88	203.0521, 147.0449, 109.0450	Cyclohexanol	+	+	+	Zhang et al., 2020
2	1.746	Vanillic acid	$C_8H_8O_4$	$[M+H]^+$ 171.0537	1.21	110.0359	Organic acids	+	+	+	Zhang et al., 2020
3	1.898	Phlorizin	$C_{21}H_{24}O_{10}$	$[M+NH_4]^+$ 454.1704	0.19	322.1277,160.0754	Flavonoids	–	+	–	Li et al.,2022
4	2.046	Quinic acid	$C_7H_{12}O_6$	$[M+H]^+$ 193.0559	1.50	131.0558, 117.0402, 103.0609	Organic acids	+	+	+	Zhang et al., 2020
5	2.200	Adoxosidic acid glycoside	$C_{22}H_{34}O_{15}$	$[M+NH_4]^+$ 556.2236	0.06	377.1436, 215.0916, 197.0805, 179.0693	Terpenes	+	–	–	Zhang et al., 2020
6	2.323	Caffeic acid 2-(1 naphthyl) bethyl ester	$C_{21}H_{18}O_4$	$[M+H]^+$ 335.1238	3.52	173.0710, 155.0597, 129.0572	Organic acids	–	+	+	Li et al.,2022
7	2.672	Galiridoside	$C_{15}H_{22}O_9$	$[M+NH_4]^+$ 364.1601	0.29	309.0915, 247.1157, 167.0700	Cyclohexanol	–	+	–	Zhou et al.,2022
8	2.749	Hydroxytyrosol glucoside	$C_{14}H_{20}O_8$	$[M+NH_4]^+$ 334.1496	0.80	155.0705, 137.0595, 109.0644, 91.0538	Phenylethanoids	+	+	+	Zhou et al.,2022
9	2.941	6′-Methoxypolygoacetophenoside	$C_{15}H_{20}O_{10}$	$[M+Na]^+$ 383.0947	1.14	221.0401, 204.0998, 185.0428	Cyclohexanol	+	+	–	Zhou et al.,2022
10	3.057	Adoxosidic acid	$C_{16}H_{24}O_{10}$	$[M+Na]^+$ 399.1271	0.11	215.0916, 197.0810, 153.0908, 105.0699	Terpenes	+	+	+	Zhang et al., 2020
11	3.290	Forsythide	$C_{16}H_{22}O_{11}$	$[M+Na]^+$ 413.1049	0.15	229.0704, 211.0602, 167.0693	Terpenes	+	+	+	Li et al.,2022
12	3.448	Vanilloloside	$C_{14}H_{20}O_8$	$[M+Na]^+$ 339.1054	0.41	137.0596	Cyclohexanol	–	+	–	
13	3.946	Salidroside	$C_{14}H_{20}O_7$	$[M+Na]^+$ 323.1099	0.17	139.0603, 121.0646	Cyclohexanol	+	+	+	Zhang et al., 2020
14	4.401	Forsythoside E	$C_{20}H_{30}O_{12}$	$[M+Na]^+$ 485.1627	0.40	317.1080, 155.0547, 137.0594	Phenylethanoids	+	+	+	Zhang et al., 2020
15	5.142	Chlorogenic acid*	$C_{16}H_{18}O_9$	$[M+H]^+$ 355.1022	0.98	163.0387, 145.0281, 135.0439, 117.0334	Organic acids	–	+	+	–
16	5.318	Forsythenside B	$C_{22}H_{26}O_{11}$	$[M+Na]^+$ 489.1355	1.10	339.1818, 321.0945, 177.0521, 159.0521	Cyclohexanol	+	+	+	Zhang et al., 2020
17	5.619	4-O-β-D-Glucosyl-4-coumaric acid	$C_{15}H_{18}O_8$	$[M+NH_4]^+$ 344.1341	1.63	165.0544, 147.0436, 119.0488	Organic acids	+	–	+	Li et al.,2022
18	5.791	Benzyl α-D-mannopyranoside	$C_{10}H_{16}O$	$[M+H]^+$ 153.1271	1.89	105.0704, 91.0549, 83.0463, 81.0688, 79.0545, 77.0386	Others	–	+	–	Zhou et al.,2022
19	5.960	Caffeic acid	$C_9H_8O_4$	$[M+H]^+$ 181.0347	0.23	137.0448, 109.0503	Organic acids	+	–	+	Chen et al., 2017
20	6.237	(3S)-3-Hydroxydecanoic acid	$C_{10}H_{20}O_3$	$[M+Na]^+$ 211.1304	0.26	143.0848	Organic acids	–	+	+	Li et al.,2022
21	6.335	Prenyl arabinosyl-(1–6)-glucoside	$C_{16}H_{28}O_{10}$	$[M+NH_4]^+$ 398.2024	1.24	380.1646, 149.0452, 119.0351, 101.0240	Others	–	+	+	Li et al.,2022
22	6.989	1-O-feruloyl-β -D-glucose	$C_{16}H_{20}O_9$	$[M+NH_4]^+$ 374.1442	0.54	195.0650, 177.0545, 146.0522, 145.0286, 117.0334	Organic acids	–	+	+	Li et al.,2022
23	7.311	p-Coumaroyl quinic acid	$C_{16}H_{18}O_8$	$[M+H]^+$ 339.1068	0.48	147.0441, 119.0492, 91.0541	Organic acids	+	+	+	Li et al.,2022
24	7.571	Hesperetin 5-O-glucoside	$C_{22}H_{24}O_{11}$	$[M+NH_4]^+$ 482.1649	1.38	447.1284, 303.0861, 191.0708, 127.0391	Flavonoids	+	+	+	Zhou et al.,2022
25	7.675	7-Epi-12-hydroxyjasmonic acid glucoside	$C_{18}H_{28}O_9$	$[M+Na]^+$ 411.16	0.55	249.0707, 167.0710	Organic acids	–	+	+	Li et al.,2022
26	7.913	Rengyoside D	$C_{22}H_{30}O_{11}$	$[M+NH_4]^+$ 488.2124	2.77	297.0962, 279.0858, 153.0542, 139.0745, 107.0489	Cyclohexanol	–	–	+	Zhang et al., 2020

(*continued on next page*)

Table 1 (*continued*)

No.	t_R (min)	Compounds	Molecular formula	Molecular ions (m/z) (mass accuracy)	Diff (ppm)	MS/MS fragments (m/z)	Classification	Fruits	Flowers	Leaves	References
27	7.969	Rengyoside C	$C_{22}H_{32}O_{10}$	$[M + Na]^+$ 479.188	3.05	263.0351, 215.0842	Cyclohexanol	–	–	+	Zhang et al., 2020
28	9.104	8-Hydroxypinoresinol 4-glucoside	$C_{26}H_{32}O_{12}$	$[M + Na]^+$ 559.1755	1.94	3731291, 343.1174, 328.0933, 313.1072	Lignans	+	+	+	Zhang et al., 2020
29	9.952	3,4-Diethoxybenzoic acid	$C_{11}H_{14}O_4$	$[M + H]^+$ 211.0964	0.46	170.0571, 155.0335, 127.0388, 114.0487	Organic acids	–	+	–	Zhou et al.,2022
30	10.707	Forsythenside A	$C_{22}H_{26}O_{10}$	$[M + Na]^+$ 473.141	0.74	315.1081, 193.0504, 175.0499, 151.0401	Cyclohexanol	+	+	+	Zhang et al., 2020
31	10.930	R-suspensaside A	$C_{29}H_{36}O_{16}$	$[M + Na]^+$ 663.1881	1.32	621.1819, 529.1561, 487.1448, 469.1376, 179.0338, 161.0233,151.0398, 135.0444	Phenylethanoids	+	+	+	Zhang et al., 2020
32	11.180	S-suspensaside A	$C_{29}H_{36}O_{16}$	$[M + Na]^+$ 663.1884	1.05	621.1819, 529.1561, 487.1448, 469.1376, 179.0338, 161.0233, 151.0398, 135.0444	Phenylethanoids	+	+	+	Zhang et al., 2020
33	11.468	(Z)-3-Hexenylvicianoside	$C_{17}H_{30}O_{10}$	$[M + Na]^+$ 417.1729	0.83	344.0973, 285.1277, 136.0822, 145.0498, 133.0490, 127.0386, 115.0390	Others	–	+	+	Zhou et al.,2022
34	11.803	Calceolarioside A	$C_{23}H_{26}O_{11}$	$[M + H]^+$ 479.1405	1.21	317.1115, 181.0349, 163.0244, 137.0450	Phenylethanoids	+	–	+	Zhang et al., 2020
35	12.536	Isolariciresinol-4-O-glucoside	$C_{26}H_{34}O_{11}$	$[M + NH_4]^+$ 540.2437	0.11	381.1532, 219.1014, 201.0918, 163.0731, 131.0847	Lignans	+	+	+	Zhou et al.,2022
36	12.560	Calceolarioside C	$C_{28}H_{34}O_{15}$	$[M + Na]^+$ 633.1788	0.60	581.1638, 547.1883, 481.0937, 453.1404, 419.0646, 383.1422, 163.0731	Phenylethanoids	+	–	–	Zhang et al., 2020
37	12.672	8-Hydroxypinoresinol-4-glucoside	$C_{26}H_{32}O_{12}$	$[M + Na]^+$ 559.1781	−0.16	357.1307, 233.0795, 203.0712, 163.0750, 131.0491	Lignans	+	–	+	Zhang et al., 2020
38	13.214	Quercetin*	$C_{15}H_{10}O_7$	$[M + H]^+$ 303.0491	0.71	285.0359, 257.0448, 229.0489, 201.0542, 165.0170, 153.0179, 137.0235	Flavonoids	+	+	+	–
39	13.214	Quercitrin	$C_{21}H_{20}O_{12}$	$[M + H]^+$ 465.1026	0.80	303.0494, 285.0405, 257.0418, 229.0491	Flavonoids	+	+	+	Li et al.,2022
40	13.701	Forsythoside I	$C_{29}H_{36}O_{15}$	$[M + H]^+$ 625.1981	1.78	463.1725, 445.1332, 317.1076, 207.0651, 181.0154, 163.0163, 137.0432	Phenylethanoids	+	+	+	Zhang et al., 2020
41	13.928	Rutin*	$C_{27}H_{30}O_{16}$	$[M + H]^+$ 611.1629	−0.26	465.1045, 303.0516, 302.0388, 273.0405, 147.0649, 129.0543	Flavonoids	+	+	+	–
42	14.241	Lariciresinol-9-glucoside	$C_{26}H_{34}O_{11}$	$[M + NH_4]^+$ 540.243	−0.72	365.0104, 219.1018, 201.0910,131.0688	Lignans	+	+	–	Zhang et al., 2020
43	14.278	Lianqiaoxinoside C	$C_{28}H_{34}O_{15}$	$[M + NH_4]^+$ 628.2221	−0.72	325.0918, 295.0808, 181.0512, 163.0389	Phenylethanoids	+	+	+	Zhang et al., 2020
44	14.512	Hyperoside	$C_{21}H_{20}O_{12}$	$[M + H]^+$ 465.1026	−0.59	303.0494, 285.0405, 257.0418, 229.0491	Flavonoids	+	+	+	Zhou et al.,2022
45	14.696	Hesperidin	$C_{28}H_{34}O_{15}$	$[M + Na]^+$ 633.1788	1.43	447.1496, 300.0281, 161.0243	Flavonoids	+	+	+	Chen et al., 2017
46	15.542	Kaempferol-3-O-rutinoside*	$C_{27}H_{30}O_{15}$	$[M + H]^+$ 595.1669	1.33	449.1120, 287.0552, 241.0502, 165.0119	Flavonoids	+	+	+	–
47	16.196	Forsythoside H	$C_{29}H_{36}O_{15}$	$[M + NH_4]^+$ 642.2386	0.01	471.1594, 325.0918, 163.0388	Phenylethanoids	+	–	–	Zhang et al., 2020
48	16.422	Forsythoside B	$C_{34}H_{44}O_{19}$	$[M + NH_4]^+$ 774.2797	−0.46	325.0914, 163.0387	Phenylethanoids	+	–	–	Zhang et al., 2020
49	16.755	Forsythoside A	$C_{29}H_{36}O_{15}$	$[M + H]^+$ 625.1893	0.73	463.1652, 445.1489, 181.0481, 163.0325, 137.0566	Phenylethanoids	+	+	+	Zhang et al., 2020

(*continued on next page*)

Table 1 (*continued*)

No.	t_R (min)	Compounds	Molecular formula	Molecular ions (*m/z*) (mass accuracy)	Diff (ppm)	MS/MS fragments (*m/z*)	Classification	Fruits	Flowers	Leaves	References
50	16.999	Forsythenside L	$C_{20}H_{28}O_{11}$	$[M+NH_4]^+$ 462.197	−0.20	151.0741	Others	+	–	+	Zhang et al., 2020
51	17.080	Calceolarioside B	$C_{23}H_{26}O_{11}$	$[M+H]^+$ 479.1401	−1.16	317.1079, 181.0350, 163.0244, 137.0452	Phenylethanoids	+	–	–	Zhang et al., 2020
52	17.304	Forsythenside H	$C_{24}H_{38}O_{10}$	$[M+Na]^+$ 509.2363	0.49	365.0529, 332.1310, 320.1467, 296.0540, 223.1099	Cyclohexanol	+	–	–	Zhang et al., 2020
53	17.436	Kaempferol	$C_{15}H_{10}O_6$	$[M+H]^+$ 287.0557	−1.00	213.0539, 185.0599, 171.0435, 165.0178, 153.0182, 107.0487	Flavonoids	–	–	+	Zhou et al.,2022
54	17.655	Pinoresinol-4-O-glucoside*	$C_{26}H_{32}O_{11}$	$[M+Na]^+$ 543.1834	0.58	381.1204, 153.0521, 138.0628	Lignans	+	+	+	–
55	19.513	Suspensaside A	$C_{29}H_{34}O_{15}$	$[M+H]^+$ 625.1824	0.71	489.1461, 461.1533, 181.0348, 163.0243, 153.0400	Phenylethanoids	+	+	+	Zhou et al.,2022
56	20.005	Epi-pinoresinol-4-O-glucoside	$C_{26}H_{32}O_{11}$	$[M+Na]^+$ 543.1832	0.46	381.1199, 153.0520, 138.0628	Lignans	+	+	+	Zhang et al., 2020
57	20.467	Acteoside	$C_{29}H_{36}O_{15}$	$[M+NH_4]^+$ 642.2379	−0.97	461.1433, 325.0921, 177.0530, 163.0385	Phenylethanoids	+	+	+	Zhang et al., 2020
58	21.665	Epi-pinoresinol-4′-O-glucoside	$C_{26}H_{32}O_{11}$	$[M+Na]^+$ 543.1834	−0.80	381.1199, 153.0520, 138.0628	Lignans	+	+	+	Zhang et al., 2020
59	23.490	Agastinol	$C_{27}H_{28}O_8$	$[M+H]^+$ 481.1853	−0.25	463.1776, 445.1635, 371.1663, 273.0750, 161.0611	Lignans	+	–	–	Zhou et al.,2022
60	23.903	Demethylphillyrin	$C_{26}H_{32}O_{11}$	$[M+NH_4]^+$ 538.228	−0.89	359.1485, 341.1379, 323.1272, 137.0594	Lignans	+	+	+	Zhang et al., 2020
61	24.330	Forsythenside K	$C_{29}H_{36}O_{14}$	$[M+NH_4]^+$ 626.2435	0.03	582.1806, 309.0971, 147.0433	Phenylethanoids	+	–	+	Zhou et al.,2022
62	25.068	2-[4-(3-Hydroxypropyl)-2-methoxyphenoxy]-1,3-propanediol 1-glucoside	$C_{19}H_{30}O_{10}$	$[M+NH_4]^+$ 436.2177	−0.15	231.0495, 153.1273, 135.1166	Others	–	+	–	Li et al.,2022
63	27.018	(+)-Pinoresinol monomethyl ether-β-D-glucoside	$C_{27}H_{34}O_{11}$	$[M+Na]^+$ 557.1992	0.02	395.1447	Lignans	+	+	+	Zhang et al., 2020
64	27.437	Suspenoidside B	$C_{25}H_{30}O_{12}$	$[M+H]^+$ 523.1659	0.54	479.1772, 361.1164, 317.1248, 299.1133, 165.0390	Lignans	+	–	–	Zhou et al.,2022
65	28.500	Matairesinoside	$C_{26}H_{32}O_{11}$	$[M+H]^+$ 521.1874	0.07	359.1336, 344.1135, 153.0399	Lignans	+	+	+	Zhou et al.,2022
66	28.906	Phillyrin*	$C_{27}H_{34}O_{11}$	$[M+Na]^+$ 557.199	2.14	371.1499, 356.1267	Lignans	+	+	+	–
67	29.511	Arctiin	$C_{21}H_{24}O_6$	$[M+H]^+$ 373.1643	−0.71	177.0904, 151.0752, 137.0597	Lignans	+	+	+	Zhou et al.,2022
68	29.512	Arctigenin	$C_{27}H_{34}O_{11}$	$[M+Na]^+$ 557.1998	−0.73	395.1488	Lignans	–	+	–	Chen et al., 2017
69	29.862	(+)-Pinoresinol	$C_{20}H_{22}O_6$	$[M+H\text{-}H_2O]^+$341.1380	0.95	291.1005, 270.0896, 211.0759, 187.0749, 137.0593	Lignans	+	+	+	Zhou et al.,2022
70	31.566	methyl (1S,2S,3S,3aR,8bS)-1-acetyloxy-8b-hydroxy-6,8-dimethoxy-3a-(4-methoxyphenyl)-3-phenyl-2,3-dihydro-1H-cyclopenta[b] (Chang et al., 2022)benzofuran-2-carboxylate	$C_{30}H_{30}O_9$	$[M+H]^+$ 535.1956	0.01	357.1344, 177.0548, 163.0747	Others	+	–	–	Li et al.,2022
71	32.650	(-)-Pinoresinol	$C_{20}H_{22}O_6$	$[M+H\text{-}H_2O]^+$341.1380	0.82	291.1005, 270.0896, 211.0759, 187.0749, 137.0593	Lignans	+	+	+	Zhou et al.,2022
72	34.143	Epipinoresinol	$C_{20}H_{22}O_6$	$[M+H]^+$ 359.1486	−0.21	341.1379, 311.1275, 205.0851, 151.0387	Lignans	+	–	–	Zhou et al.,2022
73	35.092	Matairesinol	$C_{20}H_{22}O_6$	$[M+H]^+$ 359.1485	0.26	341.1368, 311.1279, 205.0858, 151.0389	Lignans	+	–	–	Zhou et al.,2022
74	36.779	Phillygenin	$C_{21}H_{24}O_6$	$[M+H\text{-}H_2O]^+$ 355.1541	0.09	337.1438, 189.0899	Lignans	+	+	+	Chen et al., 2017

"+" detected, "-" not detected.

* Compounds identified with reference standards.

$C_9H_6O_3$-$2H_2O]^+$ (Supplementary Fig. S5). Based on the fragmentation patterns of caffeoylquinic acids, 11 organic acids including vanillic acid (2), quinic acid (4), caffeic acid 2-(1 naphthyl) bethyl ester (6), chlorogenic acid (15), 4-O-β-D-glucosyl-4-coumaric acid (17), caffeic acid (19), (3S)-3-hydroxydecanoic acid (20), 1-O-feruloyl-β-D-glucose (22), p-coumaroyl quinic acid (23), 7-epi-12-hydroxyjasmonic acid glucoside (25) and 3,4-diethoxybenzoic acid (29) were identified or tentatively identified.

For flavonoids, rutin could be an example. Rutin exhibited the precursor ion $[M + H]^+$ at *m/z* 611.1629 ($C_{27}H_{30}O_{16}$) in MS/MS spectrum (Supplementary Fig. S6), and produce ions at *m/z* 465.1045 $[M + H\text{-}C_6H_{10}O_4]^+$, 303.0516 $[M + H\text{-}C_6H_{10}O_5\text{-}C_6H_{10}O_4]^+$, 302.0388 $[M + H\text{-}C_6H_{10}O_5\text{-}C_6H_{10}O_4\text{-}H]^+$, 273.0405 $[M + H\text{-}C_6H_{10}O_5\text{-}C_6H_{10}O_4\text{-}CH_2O]^+$ by loss of glucose, rhamnose and CH_2O. In addition, the RDA cleavage-related ions at *m/z* 153.0218 $[RDA]^+$ were also observed. A total of 9 flavonoids, such as phlorizin (3), hesperetin 5-O-glucoside (24), quercetin (39), quercitrin (39), rutin (41), hyperoside (44), hesperidin (45), kaempferol-3-O-rutinoside (46), kaempferol (53) have been identified in FS.

It has been widely reported that secondary metabolites of FS were dominated by phenylethanoid glycosides, lignans and cyclohexanol derivatives. However, various organic acids and flavonoids have been also detected in different parts of FS. Based on the chemical characterization results, it could be noted that the chemical profiles of secondary metabolites in fruits, flowers and leaves were similar, but there were still certain different constituents among the different parts of FS samples (Dong et al., 2017). Four phenylethanoid glycosides, including calceolarioside C (36), forsythoside H (47), forsythoside B (48), calceolarioside B (51), and four lignans, including agastinol (59), suspenoidside B (64), epipinoresinol (72), matairesinol (73) were only contained in fruits of FS. Several metabolites, such as phlorizin (3), galiridoside (7), vanilloloside (12), 3,4-diethoxybenzoic acid (29), arctigenin (68) were only detected in flowers of FS. The leaves of FS also contained some unique secondary metabolites, such as rengyoside D (26) and rengyoside C (27), two cyclohexanol derivatives.

3.2. Chemical comparison of different parts of Forsythia suspensa by metabolomics analysis

To further explore the distribution of secondary metabolites and characterize differential metabolites among the fruits, leaves and flowers of FS, plant metabolomics analysis was performed on UPLC-QTOF-MS/MS data. Multivariate statistical analysis including PCA and OPLS-DA were employed to compare and investigate the secondary metabolites difference of the three parts of FS.

PCA is an unsupervised multivariate statistical method that can examine correlations among multiple variables, and enable data simplification and visualization (Chen et al., 2022). In order to fully understand the aggregation and dispersion differences among fruits, leaves and flowers of FS, PCA was performed on the relative abundance of 74 secondary metabolites identified by UPLC-QTOF-MS/MS. The results of PCA display the metabolic differences and similarities among the different samples. As shown in Fig. 3A, the green dots, red dots, blue dots and yellow dots represented the fruits, leaves, flowers and QC samples, respectively. The R^2X (Chang et al., 2022), R^2X (Chang et al., 2021) and Q^2 parameters of the PCA model were 0.326, 0.216 and 0.914, which indicated a receivable classification and prediction ability of the model. The score plot of PCA showed that the QC samples were tightly clustered in the center as one cluster, which indicated that the analytic system was stable. 40 batches of different parts of FS samples could be clearly divided into three clusters corresponding to fruits, leaves and flowers of FS. It could be noted that the fruits and flowers samples were relatively concentrated, which indicated relatively smaller within-group differences of the samples. While the leaves samples were relatively evacuated, indicating larger within-group differences. In general, the difference among the fruits, leaves and flowers of FS samples were obvious and differentiated, and the PCA results indicated that the secondary metabolites among the fruits, leaves, flowers of FS were significant different.

OPLS-DA is a supervised multivariate statistical method which focuses on the differentiation between groups, and a reliable tool to screen of differential metabolites (Jin et al., 2021). The OPLS-DA model could achieve effective separation of samples with little differences, and identify the characteristic variables for distinction. Thus, OPLS-DA was further employed to compare the secondary metabolites difference and find the potential differential metabolites among the fruits, leaves and flowers of FS. The OPLS-DA results showed that the R^2Y and Q^2 of the established model were 0.994 and 0.957, and there was no overfitting or outliers when the outputs of the permutation test ($N = 200$) and the Hotelling T2 test (using 95 % and 99 % confidence limits) were examined, which indicating the OPLS-DA model had a great classification and prediction ability. The score plot of OPLS-DA (Fig. 3B) showed that the three different parts of FS samples were clearly concentrated in three regions, which was consistent with the results of PCA. To select the differential metabolites, the secondary metabolites identified in different parts of FS were further screened based on VIP values. The VIP values represent the differences of the variables, and variables could be regard as important roles for the differentiation when the VIP values were more than 1.5 (Li et al., 2024). Thus, the VIP values of the secondary metabolites were further calculated to select the potential differential metabolites among the different parts of FS samples. Finally, a total of 29 secondary metabolites were screened out as the potential differential metabolites based on the condition of VIP > 1.5, $P < 0.05$ (Supplementary Table S2). The results showed that the 29 potential differential metabolites including 5 phenylethanol glycosides, 8 lignans, 5 cyclohexanol derivatives, 4 flavonoids, 4 organic acids, 1 triterpene,

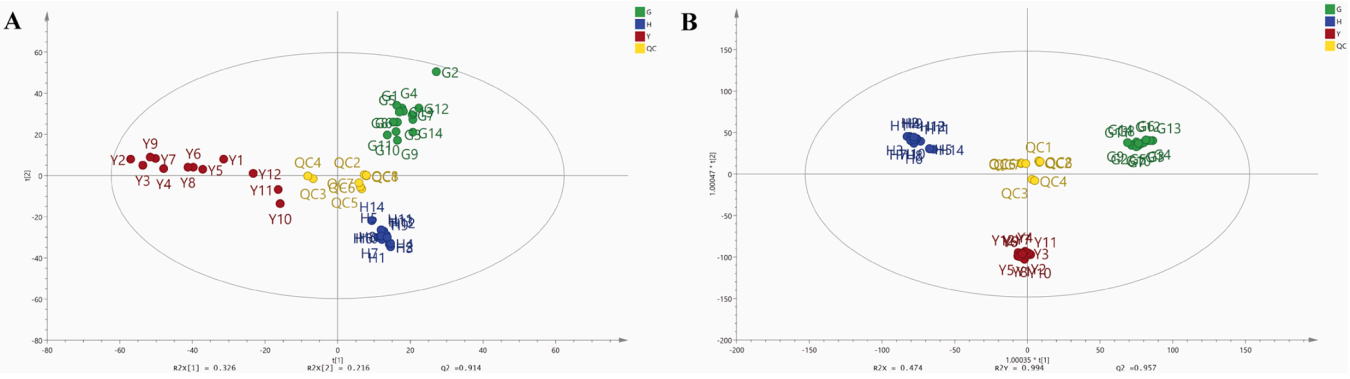

Fig. 3. The score plots of PCA (A) and OPLS-DA (B) of fruits, flowers and leaves of *Forsythia suspensa* samples. Fruits, G1-G14; Flowers, H1-H14; Leaves, Y1-Y12; Quality control, QC1-QC8.

and 2 other components were significant to effectively discriminate the fruits, leaves and flowers of FS samples, and these characteristic metabolites could be recognized as chemical markers for discrimination and difference of the three different parts of FS.

Then, a clustering heatmap analysis was established to reveal the distribution of 29 screened differential metabolites. As shown in Fig. 4, 40 batches of different parts of FS samples were divided into three groups corresponding to fruits, leaves, flowers based on the relative abundance of the differential metabolites. It could obviously find that the distribution of 29 secondary metabolites in fruits, leaves, flowers of FS differed greatly, which indicated that the relative contents of these metabolites were different. The relative contents of forsythoside I (40), pinoresinol-4-O-glucoside (54), epipinoresinol (72) and matairesinol (73) were higher in fruits of FS compared to those of flowers and leaves. Compared to fruits and leaves, the relative contents of caffeic acid 2-(1-naphthyl) ethyl ester (6), galiridoside (7), vanilloloside (12), 2-[4-(3-hydroxypropyl)-2-methoxyphenoxy]-1,3-propanediol-1-glucoside (62) and (+)-pinoresinol monomethyl ether-β-D-glucoside (63) were higher in flowers of FS. While the relative contents of rengynic acid-4-O-β-D-glucoside (1), forsythoside E (14), forsythenside A (30), (Z)-3-hexenylvicianoside (33), 8-hydroxypinoresinol-4-glucoside (37), kaempferol-3-O-rutinoside (46), forsythoside A (49), phillyrin (66) and phillygenin (74) of leaves samples were much higher than those of the fruits and flowers samples.

3.3. α-Glucosidase and pancreatic lipase inhibitory activities of different parts of Forsythia suspensa

The α-glucosidase inhibitors can reduce glucose in dietary carbohydrates and lower postprandial blood glucose, which are helpful in reducing post-prandial blood glucose in treating prediabetic conditions and delaying the progression of diabetes (Hasan et al., 2023). Pancreatic lipase can involve in the absorption of dietary lipids in the gastrointestinal tract, and the pancreatic lipase inhibitors could prevent the hydrolytic absorption of fat (Zeng et al., 2018). In this present work, the α-glucosidase and pancreatic lipase inhibitory activities of fruits, leaves and flowers of FS samples have been studied by α-glucosidase and pancreatic lipase inhibition assays *in vitro*. Acarbose and orlistat were used as positive controls in α-glucosidase and pancreatic lipase inhibition assays, respectively. The results showed that acarbose had great inhibitory effect on α-glucosidase with the IC_{50} 0.019 ± 0.001 μmol/mL and orlistat also exhibited good inhibitory effect on pancreatic lipase with the IC_{50} 0.086 ± 0.016 μmol/mL, which indicated the established α-glucosidase and pancreatic lipase inhibition assays were reliable. As shown in Fig. 5A, all the different parts of FS samples displayed good α-glucosidase inhibitory activities, but the IC_{50} of fruits, leaves and flowers of FS samples were different. The average IC_{50} values of the fruits, leaves and flowers of FS samples on α-glucosidase were 0.24 ± 0.06 mg/mL, 0.17 ± 0.04 mg/mL, and 0.41 ± 0.10 mg/mL, respectively (Fig. 5B). For pancreatic lipase, all the different parts of FS samples also displayed good inhibitory activities (Fig. 5C), and the average IC_{50} values of the fruits, leaves and flowers of FS samples were 0.94 ± 0.23 mg/mL 0.56 ± 0.33 mg/mL, 0.65 ± 0.15 mg/mL, respectively (Fig. 5D). The α-glucosidase and pancreatic lipase inhibition results showed that the leaves of FS had the strongest α-glucosidase and pancreatic lipase inhibitory capacities among the three parts of FS samples, which the IC_{50} values were 0.17 ± 0.04 mg/mL and 0.56 ± 0.33 mg/mL, respectively.

The results of α-glucosidase and pancreatic lipase inhibition assays demonstrated that all the fruits, leaves and flowers of FS have significant medicinal potential in inhibiting α-glucosidase and pancreatic lipase, and the inhibitions of different parts of FS varied greatly. The different inhibitory effects of α-glucosidase inhibition and pancreatic lipase could be due to the presence of characteristic metabolites in different parts of FS samples. Further research is needed to investigated the relationships between the characteristic metabolites and α-glucosidase and pancreatic lipase inhibitory activities, and explore the potential α-glucosidase and pancreatic lipase inhibitory constituents.

3.4. Pearson correlation analysis

In order to further investigate the relevance between characteristic metabolites and enzyme inhibitory activities, Pearson correlation analysis was employed. Pearson correlation analysis is a multivariate statistical model, which is applied to extract factors that have the greatest impact on the outcome variables and maximize the relationships between the two sets of variables (Zhang et al., 2023). In this present work, the abundance of 29 differential metabolites and IC_{50} of enzymes

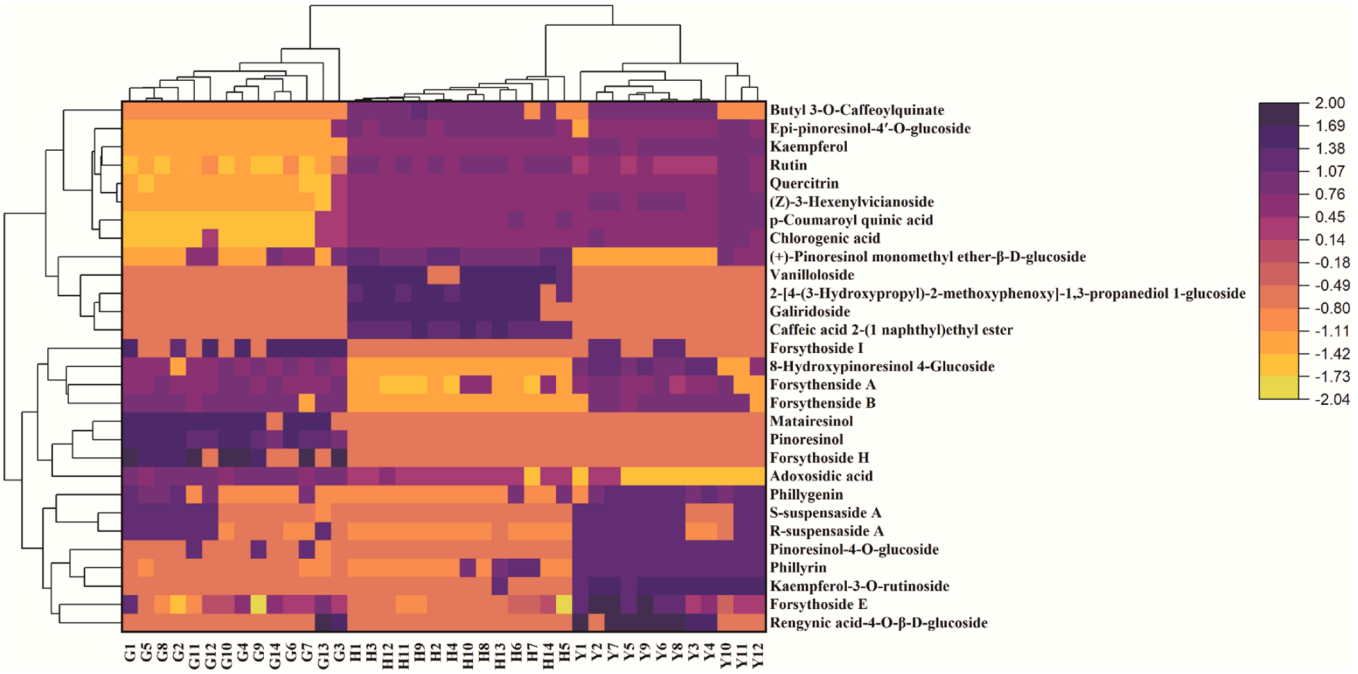

Fig. 4. Heatmap analysis of 29 different metabolites in fruits, flowers and leaves of *Forsythia suspensa*. Fruits, G1-G14; Flowers, H1-H14; Leaves, Y1-Y12.

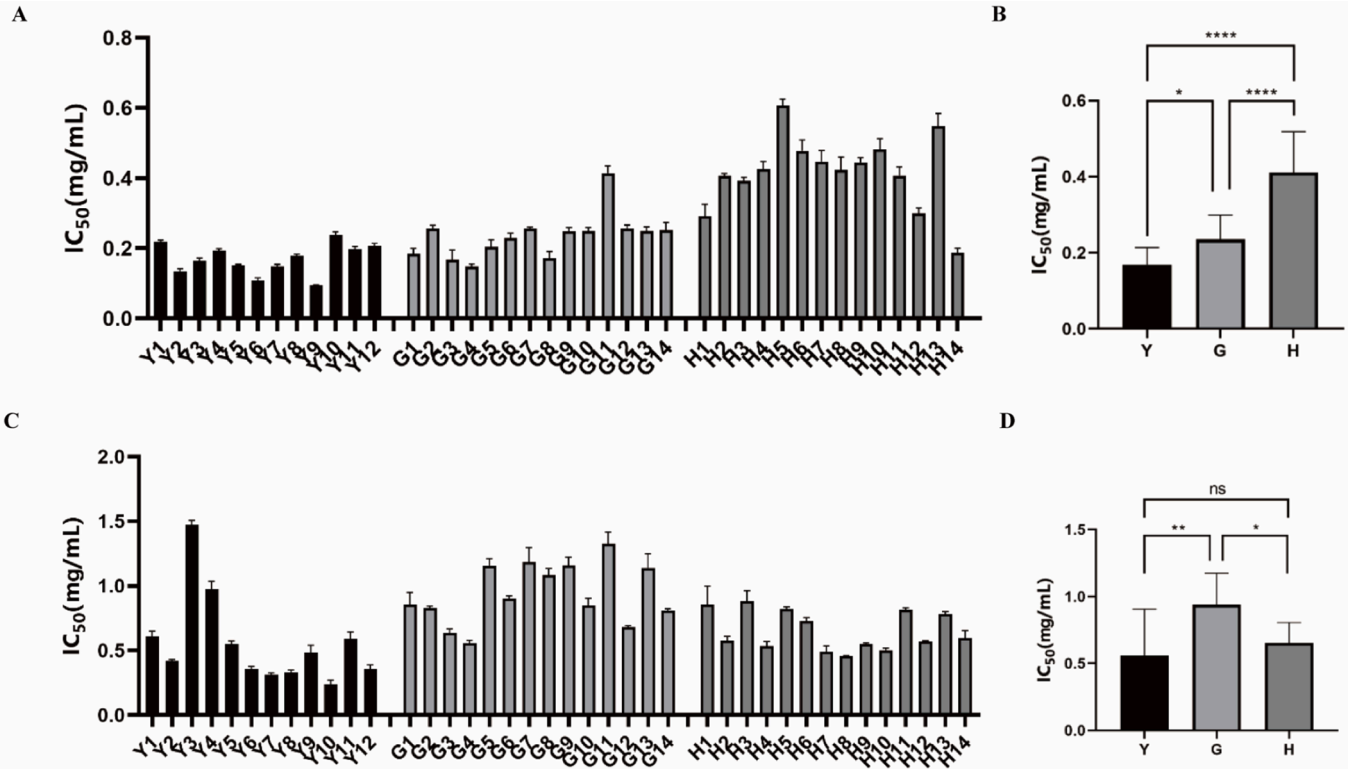

Fig. 5. The inhibitory activities of fruits, flowers and leaves of *Forsythia suspensa* on α-glucosidase and pancreatic lipase. (A) The IC_{50} values of different batches of fruits (G1-G14), flowers (H1-H14) and leaves (Y1-Y12) of *Forsythia suspensa* on α-glucosidase. (B) The average IC_{50} values of fruits (G), flowers (F) and leaves (L) of *Forsythia suspensa* samples on α-glucosidase. (C) The IC_{50} values of different batches of fruits (G1-G14), flowers (H1-H14) and leaves (Y1-Y12) of *Forsythia suspensa* samples on pancreatic lipase. (D) The average IC_{50} values of fruits (G), flowers (F) and leaves (L) of *Forsythia suspensa* samples on pancreatic lipase. $^{*}P < 0.05$, $^{**}P < 0.01$.

(α-glucosidase or pancreatic lipase) inhibitory capacities of fruits, leaves and flowers of FS samples were set as two groups of variables, and the Pearson correlation coefficients between these two groups were calculated. As shown in Fig. 6, among the 29 differential metabolites screened above, 15 metabolites were negatively correlated with α-glucosidase inhibition activity, and 21 metabolites were negatively correlated with pancreatic lipase inhibition activity. It could be observed (Table 2) that 12 characteristic metabolites including rengynic acid-4-O-β-D-glucoside (1), forsythoside E (14), 8-hydroxypinoresinol-4-glucoside (28), forsythenside A (30), R-suspensaside A (31), S-suspensaside A (32), quercitrin (38), rutin (41), kaempferol-3-O-rutinoside (46), pinoresinol-4-O-glucoside (54), phillyrin (66), phillygenin (74) were negatively correlated to both the two enzyme inhibitory activities, which indicated that these 12 metabolites had high inhibitory effects on both α-glucosidase and pancreatic lipase, and the inhibitory activities of the samples for both enzymes increased with the increase in the content of these components.

Pearson correlation analysis results showed that some certain components in different parts of FS had significant contribution to α-glucosidase and pancreatic lipase inhibitory activities, and could be recognized as potential enzyme inhibitory ingredients. Finally, a total of 12 characteristic metabolites were screen out as potential α-glucosidase and pancreatic lipase inhibitors in different parts of FS.

3.5. Validation of α-glucosidase and pancreatic lipase inhibitors in vitro

According to the results of Pearson correlation analysis, 12 potential α-glucosidase and pancreatic lipase inhibitors have been explored in FS. In order to verify the reliability of the result, the α-glucosidase and pancreatic lipase inhibitory activities of 5 potential inhibitors including quercitrin, rutin, kaempferol-3-O-rutinoside, pinoresinol-4-O-glucoside and phillyrin were determined by α-glucosidase and pancreatic lipase inhibition assays *in vitro*. As shown in Fig. 7, all the five components displayed strong inhibitory effects on α-glucosidase and pancreatic lipase in concentration dependent manners. For α-glucosidase inhibitory activity, the IC_{50} of quercitrin, rutin, kaempferol-3-O-rutinoside, pinoresinol-4-O-glucoside, and phillyrin were 0.162 ± 0.004 μmol/mL, 0.072 ± 0.004 μmol/mL, 0.101 ± 0.001 μmol/mL, 1.206 ± 0.082 μmol/mL, 0.515 ± 0.002 μmol/mL, respectively. For pancreatic lipase inhibitory activity, the IC_{50} of quercitrin, rutin, kaempferol-3-O-rutinoside, pinoresinol-4-O-glucoside, and phillyrin were 0.215 ± 0.018 μmol/mL, 0.135 ± 0.009 μmol/mL, 0.105 ± 0.006 μmol/mL, 2.685 ± 0.197 μmol/mL, and 1.614 ± 0.114 μmol/mL, respectively. The above results indicated that the selected potential enzymes inhibitors have certain α-glucosidase and pancreatic lipase inhibition, which verified the results of Pearson correlation analysis.

3.6. Molecular docking analysis

In order to further verify the α-glucosidase and pancreatic lipase inhibitory activities of the five enzyme inhibitors mentioned above and predict the preferred binding sites, molecular docking models were constructed. The predicted binding modes of the five enzyme inhibitors docked into α-glucosidase are shown in Fig. 8. The Prime module of the Schrodinger software was used to calculate the free energy of binding between the five small molecule ligands and the α-glucosidase protein (3A4A). The optimal binding affinities of quercitrin, rutin, kaempferol-3-O-rutinoside, pinoresinol-4-O-glucoside, and phillyrin were −9.91 kcal/mol, −10.0544 kcal/mol, −10.4045 kcal/mol, −8.53959 kcal/mol and −9.29068 kcal/mol, respectively. The molecular docking results indicated that all the five small molecule compounds could bind α-glucosidase protein well, and kaempferol-3-O-rutinoside had the best

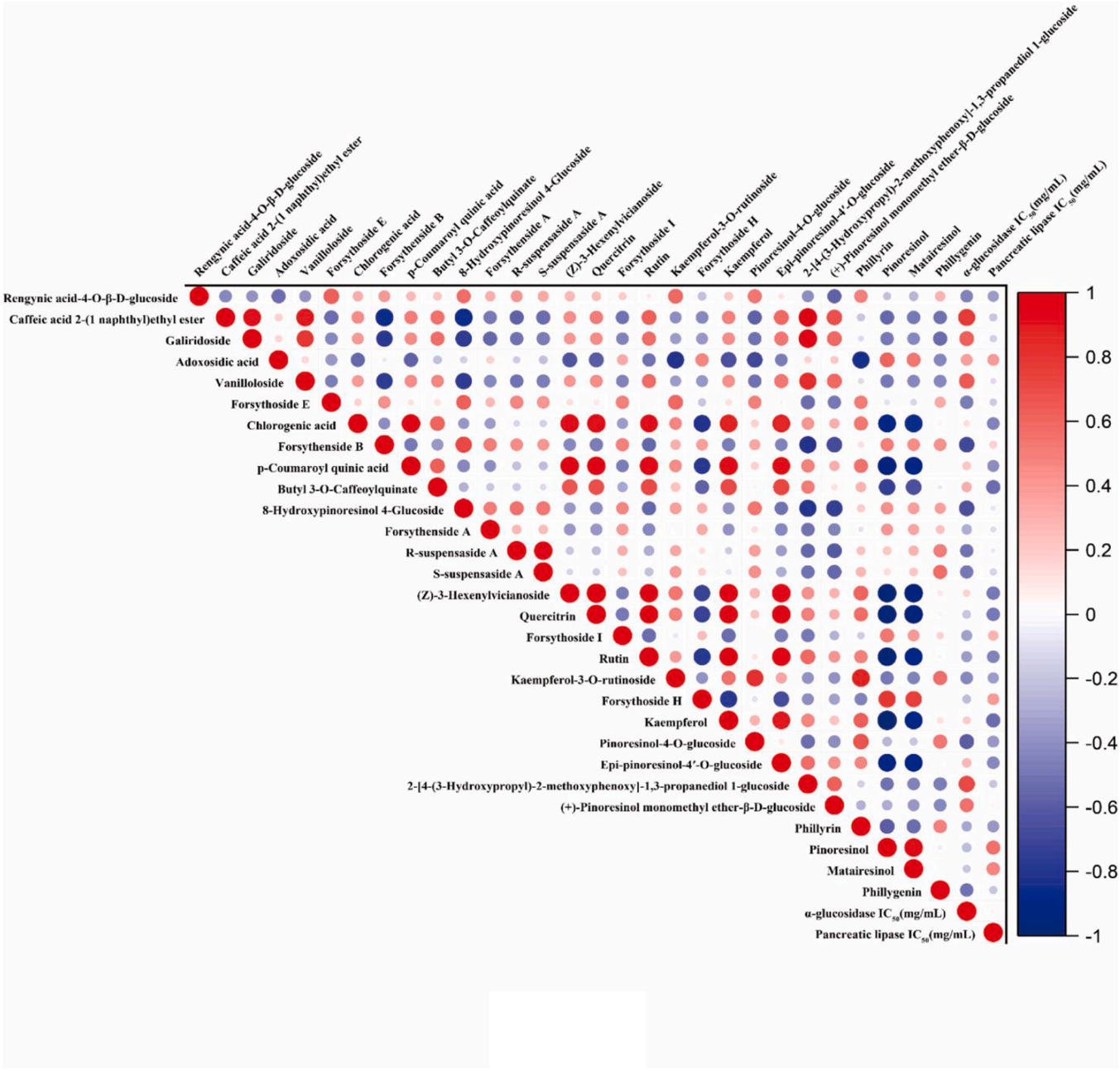

Fig. 6. Pearson correlation analysis between 29 differential metabolites and α-glucosidase and pancreatic lipase inhibitory activities (IC_{50} values). Red means positive correlation and blue means negative correlation. (For interpretation of the references to colour in this figure legend, the reader is referred to the web version of this article.)

binding effect, which was consistent with the trend of inhibitory capacities of the five compounds against α-glucosidase (IC_{50} values). Kaempferol-3-O-rutinoside formed hydrogen bonds with LYS-156, SER-240, SER241, THR-310, ASP-307, ASP-352, ARG-315, GLU-277 residues, Pi-Pi interactions with residue TYR-158, and hydrophobic bonds with GLU-411 and TYR-158 residues of α-glucosidase protein. Similarly, the quercitrin, rutin, pinoresinol-4-O-glucoside and phillyrin also formed hydrogen bonds, ionic bonds and hydrophobic interactions with multiple residues of α-glucosidase protein. LYS-156 and GLU277 residues contributed the most to protein and ligand interactions.

The predicted binding modes of the five enzyme inhibitors docked into pancreatic lipase were also investigated (Fig. 9). The free energy of binding between the five small molecule ligands and the pancreatic lipase protein (1LPB) was calculated by the same method as above. The optimal binding affinity of quercitrin, rutin, kaempferol-3-O-rutinoside, pinoresinol-4-O-glucoside, and phillyrin and pancreatic lipase were −8.97 kcal/mol, −9.96 kcal/mol, −10.01 kcal/mol, −8.0428 kcal/mol and −9.56 kcal/mol, which indicated that these small molecule compounds and pancreatic lipase had relatively ideal potential activity effects. Among the five enzyme inhibitors, kaempferol-3-O-rutinoside had the best binding effect, which was basically consistent with the trend of the verification results of pancreatic lipase inhibitory activities *in vitro*. Kaempferol-3-O-rutinoside formed hydrogen bonds with PHE-77, ASP-79, ARG-256, THR-255, SER-152 residues and Pi-Pi interactions with PHE-215 residues of pancreatic lipase protein. The quercitrin, rutin, pinoresinol-4-O-glucoside and phillyrin also formed hydrogen bonds, ionic bonds and hydrophobic interactions with multiple residues of pancreatic lipase protein, such as PHE-215, ARG-256 and ASP-79.

Table 2
Pearson correlation coefficients between differential metabolites and inhibitory activities of α-glucosidase and pancreatic lipase.

Metabolites	Coefficients (r)	
	α-Glucosidase	Pancreatic lipase
Rengynic acid-4-O-β-D-glucoside	−0.4515	−0.3528
Caffeic acid 2-(1 naphthyl) ethyl ester	0.7707	−0.1800
Galiridoside	0.6343	−0.14404
Adoxosidic acid	0.3767	0.3938
Vanilloloside	0.6572	−0.1075
Forsythoside E	−0.4713	−0.1624
Chlorogenic acid	0.1245	−0.4556
Forsythenside B	−0.6814	0.1688
p-Coumaroyl quinic acid	0.2117	−0.4019
Butyl 3-O-caffeoylquinate	0.3083	−0.5394
8-Hydroxypinoresinol 4-glucoside	−0.6563	−0.0691
Forsythenside A	−0.2879	−0.1082
R-suspensaside A	−0.5044	−0.0621
S-suspensaside A	−0.4840	−0.1394
(Z)-3-Hexenylvicianoside	0.1600	−0.4887
Quercitrin	−0.2059	−0.4943
Forsythoside I	−0.3204	0.2832
Rutin	−0.3372	−0.4557
Kaempferol-3-O-rutinoside	−0.4364	−0.3515
Forsythoside H	−0.2239	0.3826
Kaempferol	0.1990	−0.5389
Pinoresinol-4-O-glucoside	−0.5996	−0.3678
Epi-pinoresinol-4′-O-glucoside	0.2719	−0.4309
2-[4-(3-Hydroxypropyl)-2-methoxyphenoxy]-1,3-propanediol 1-glucoside	0.7036	−0.1808
(+)-Pinoresinol monomethyl ether -β-D-glucoside	0.5523	0.0505
Phillyrin	−0.3179	−0.3740
Pinoresinol	−0.2378	0.5413
Matairesinol	−0.1942	0.4685
Phillygenin	−0.5168	−0.1873

In summary, the molecular docking results indicated that the five potential enzyme inhibitors in FS mainly compete with the substrate for the active sites of α-glucosidase and pancreatic lipase through hydrogen bonding, hydrophobic forces and ionic bonding to achieve inhibition of enzyme activities.

4. Conclusions

In this study, the secondary metabolites of different parts (fruits, leaves and flowers) of FS were characterized and compared for the first time using UPLC-QTOF-MS/MS combined with plant metabolomic analysis. A total of 74 secondary metabolites, including 15 phenylethanoid glycosides, 20 lignans, 10 cyclohexanol derivatives, 11 organic acids, 9 flavonoids, 3 triterpenes, and 10 other compounds were identified in three different parts of FS. A total of 29 secondary metabolites were screened out as the potential differential metabolites by multivariate statistical analysis and could be used to distinguish and differentiate the fruits, leaves and flowers of FS. The α-glucosidase and pancreatic lipase inhibitory activities of the three parts of FS samples were also analyzed. The results indicated that the inhibitions of different parts of FS varied greatly, and leaves had the highest inhibitory effects on α-glucosidase and pancreatic lipase. Pearson correlation coefficients between α-glucosidase and pancreatic lipase inhibitory activities and the screened differential metabolites was further investigated, and 12 potential α-glucosidase and pancreatic lipase inhibitory components were screen. Additionally, molecular docking analysis was carried out to explore the inhibitory mechanisms of the potential inhibitors on α-glucosidase and pancreatic lipase. In conclusion, this present study could facilitate better understanding of chemical difference of fruits, leaves and flowers of FS and provide evidences for the α-glucosidase and pancreatic lipase inhibitory activities. The results also provide useful information for future utilization of FS in pharmaceutical and food fields.

CRediT authorship contribution statement

Yan-Li Ji: Data curation, Methodology, Writing - original draft. **Xie Feng:** Investigation, Visualization, Writing - original draft. **Ya-Qing Chang:** Validation. **Yu-Guang Zheng:** Resources. **Fang-Jie Hou:** Conceptualization, Resources, Validation. **Dan Zhang:** Conceptualization, Project administration. **Long Guo:** Conceptualization, Writing - review & editing.

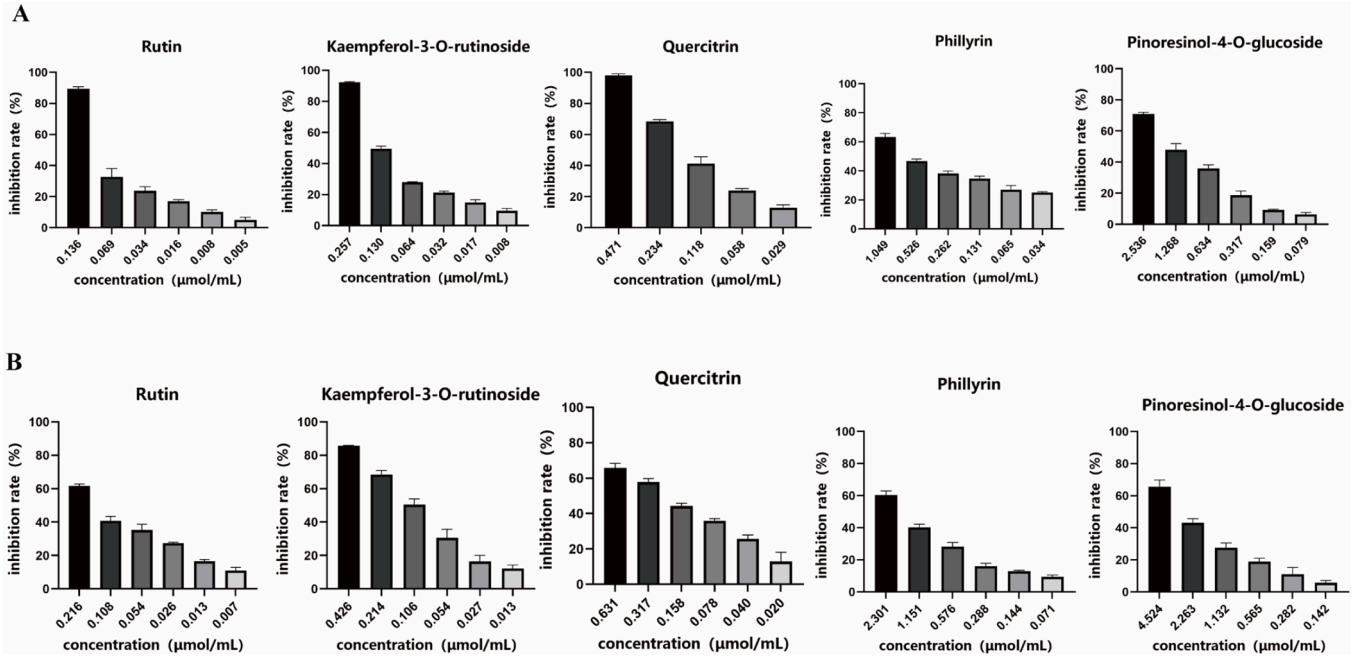

Fig. 7. Inhibitory effects of quercitrin, rutin, kaempferol-3-O-rutinoside, pinoresinol-4-O-glucoside and phillyrin on α-glucosidase (A) and pancreatic lipase (B).

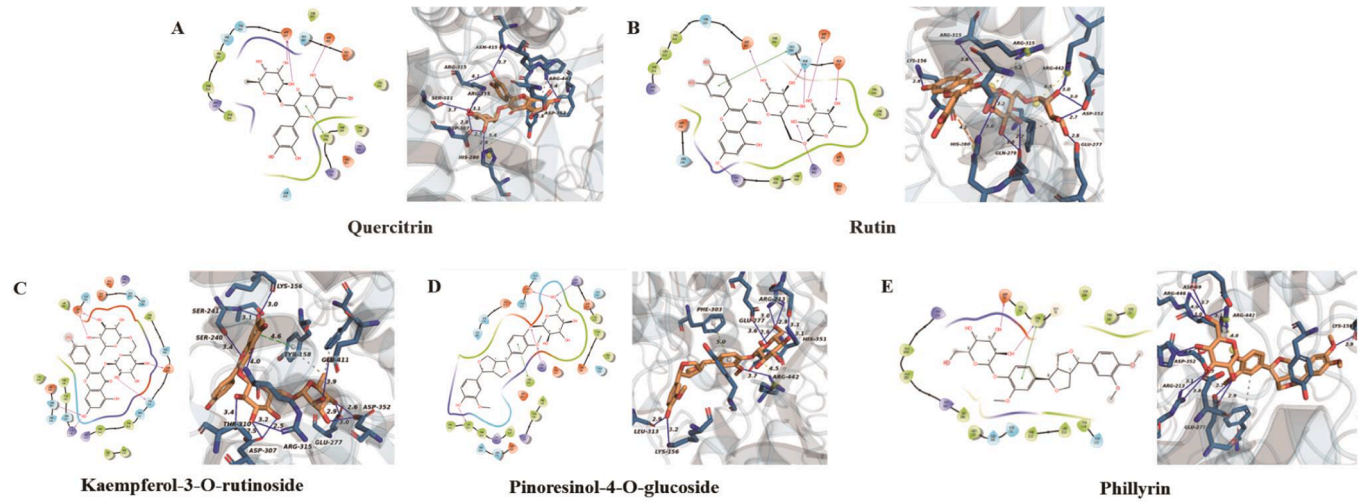

Fig. 8. The molecular docking analysis of five enzyme inhibitors with α-glucosidase protein receptor (3A4A). (A) quercitrin, (B) rutin, (C) kaempferol-3-O-rutinoside, (D) pinoresinol-4-O-glucoside, (E) phillyrin.

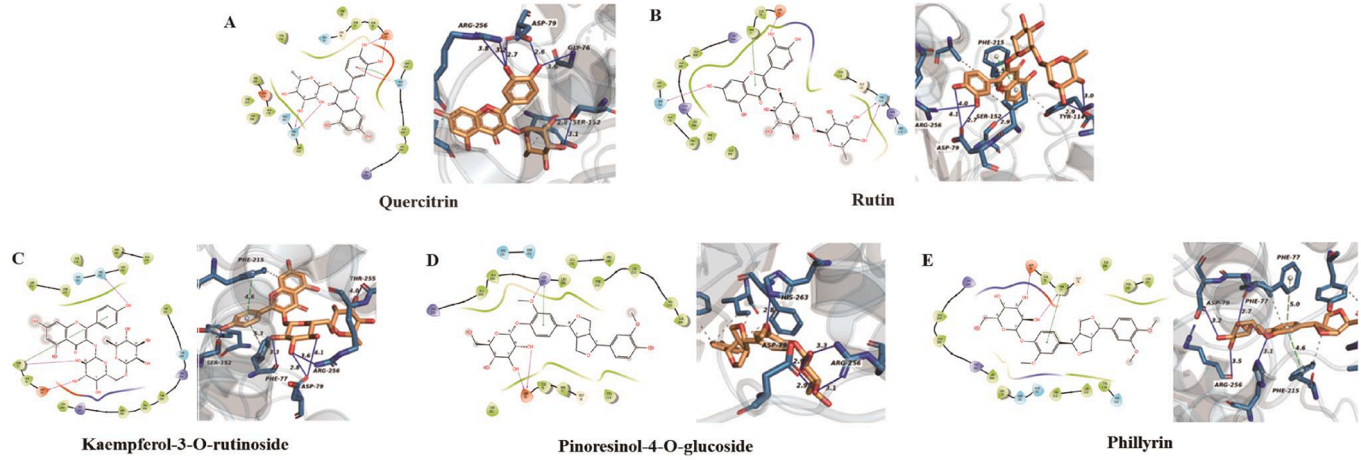

Fig. 9. The molecular docking analysis of five enzyme inhibitors with pancreatic lipase protein receptor (1LPB). (A) quercitrin, (B) rutin, (C) kaempferol-3-O-rutinoside, (D) pinoresinol-4-O-glucoside, (E) phillyrin.

Declaration of competing interest

The authors declare that they have no known competing financial interests or personal relationships that could have appeared to influence the work reported in this paper.

Acknowledgements

This work was supported by Natural Science Foundation of Hebei Province (H2021423004, H2022418001), S&T Program of Hebei Province (223777127D, 22372503D), The Central Guidance on Local Science and Technology Development Fund of Hebei Province (226Z7714G), Research Foundation of Hebei Provincial Administration of Traditional Chinese Medicine (Z2022019, 2022100).

Appendix A. Supplementary data

Supplementary data to this article can be found online at https://doi.org/10.1016/j.arabjc.2024.105723.

References

Chang, Y.Q., Zhang, D., Yang, G.Y., et al., 2021. Screening of anti-lipase components of Artemisia argyi leaves based on spectrum-effect relationships and HPLC-MS/MS. Front. Pharmacol. 12, 675396 https://doi.org/10.3389/fphar.2021.675396.

Chang, Y.Q., Fan, W.X., Shi, H., et al., 2022. Characterization of phenolics and discovery of α-glucosidase inhibitors in Artemisia argyi leaves based on ultra-performance liquid chromatography-tandem mass spectrometry and relevance analysis. J. Pharm. Biomed. Anal. 220, 114982 https://doi.org/10.1016/j.jpba.2022.114982.

Chen, Y.Q., F, X.S., Zhou, L.P., et al, 2022. Screening and evaluation of quality markers from Shuangshen Pingfei formula for idiopathic pulmonary fibrosis using network pharmacology and pharmacodynamic, phytochemical, and pharmacokinetic analyses. Phytomedicine. 100, 154040. doi:10.1016/j.phymed.2022.154040.

Chen, T.G., Li, Y.Y., Zhang, L.W., 2017. Nine different chemical species and action mechanisms of pancreatic lipase ligands screened out from Forsythia suspensa leaves all at one time. Molecules 22, 795. https://doi.org/10.3390/molecules22050795.

Chinese Pharmacopoeia Commission, 2020. Pharmacopoeia of the People's Republic of China. China Medical Science and Technology Press, Beijing, p. 177.

Cui, L., Lu, H., Lee, Y.H., 2018. Challenges and emergent solutions for LC-MS/MS based untargeted metabolomics in diseases. Mass Spectrom. Rev. 37, 772–792. https://doi.org/10.1002/mas.21562.

Darwish, R.S., El-Banna, A.A., Ghareeb, D.A., et al., 2022. Chemical profiling and unraveling of anti-COVID-19 biomarkers of red sage (Lantana camara L.) cultivars using UPLC-MS/MS coupled to chemometric analysis, in vitro study and molecular docking. J. Ethnopharmacol. 291, 115038 https://doi.org/10.1016/j.jep.2022.115038.

Dong, Z., Lu, X., Tong, X., et al., 2017. Forsythiae fructus: a review on its phytochemistry, quality control, pharmacology and pharmacokinetics. Molecules 22, 1466. https://doi.org/10.3390/molecules22091466.

Ge, Y., Wang, Y.Z., Chen, P.P., et al., 2016. Polyhydroxytriterpenoids and phenolic constituents from Forsythia suspensa (thunb.) vahl leaves. J. Agric. Food Chem. 64, 125–131. https://doi.org/10.1021/acs.jafc.5b04509.

Hasan, T., Islam, A., Riva, R., et al., 2023. Phytochemicals from Zingiber capitatum rhizome as potential α-glucosidase, α-amylase, and glycogen phosphorylase inhibitors for the management of type-II diabetes mellitus: inferences from in vitro, in vivo and in-silico investigations. Arab. J. Chem. 16, 105128 https://doi.org/10.1016/j.arabjc.2023.105128.

Jia, J.P., Zhang, F.S., Li, Z.Y., et al., 2015. Comparison of fruits of Forsythia suspensa at two different maturation stages by NMR-based metabolomics. Molecules 20, 10065–10081. https://doi.org/10.3390/molecules200610065.

Jin, T.T., Liu, F.J., Jiang, Y., et al., 2021. Molecular-networking-guided discovery of species-specific markers for discriminating five medicinal Paris herbs. Phytomedicine 85, 153542. https://doi.org/10.1016/j.phymed.2021.153542.

Kandida, I., Tari, M., Fatiqin, A. 2023. Effectiveness of the combination of green betel leaf extract (Piper betle) and mint leaf (Mentha piperita) as antibacterials against streptococcus mutans. Bioactivities 1, 32-38. . 2963-654X.184.

Kuo, P.C., Hung, H.Y., Nian, C.W., et al., 2017. Chemical constituents and anti-inflammatory principles from the fruits of Forsythia suspensa. J. Nat. Prod. 80, 1055–1064. https://doi.org/10.1021/acs.jnatprod.6b01141.

Kurniawan, Y.S., Indriani, T., Amrulloh, H., et al., 2023. The journey of natural products: from isolation stage to drug's approval in clinical trials. Bioactivities 1, 43–60. https://doi.org/10.47352/bioactivities.2963-654X.190.

Li, C., Sun, C.Z., Yang, Y.H., et al., 2022. A novel strategy by integrating chemical profiling, molecular networking, chemical isolation, and activity evaluation to target isolation of potential anti-ACE2 candidates in forsythiae fructus. Phytomedicine 96, 153888. https://doi.org/10.1016/j.phymed.2021.153888.

Li, S.B., Tian, Y.F., Jiang, P.Y.Z., et al., 2020. Recent advances in the application of metabolomics for food safety control and food quality analyses. Crit. Rev. Food Sci. Nutr. 61, 1448–1469. https://doi.org/10.1080/10408398.2020.1761287.

Li, Z.T., Zhang, F.X., Fan, C.L., et al., 2021. Discovery of potential Q-marker of traditional chinese medicine based on plant metabolomics and network pharmacology: periplocae cortex as an example. Phytomedicine 85, 153535. https://doi.org/10.1016/j.phymed.2021.153535.

Li, C., Zou, Y., Liao, G., et al., 2024. Identification of characteristic flavor compounds and small molecule metabolites during the ripening process of nuodeng ham by GC-IMS, GC-MS combined with metabolomics. Food Chem. 440, 138188 https://doi.org/10.1016/j.foodchem.2023.138188.

Pan, M.H., Su, Y.F., Liu, X.J., et al., 2022. Identification of Forsythia suspensa (thunb.) vahl in different harvest periods using intelligent sensory technologies, HPLC characteristic fingerprint coupled with chemometrics. Phytochem. Anal. 33, 490–501. https://doi.org/10.1002/pca.3104.

Salem, M.A., El-Shiekh, R.A., Aborehab, N.M., et al., 2023. Metabolomics driven analysis of Nigella sativa seeds identifies the impact of roasting on the chemical composition and immunomodulatory activity. Food Chem. 398, 133906 https://doi.org/10.1016/j.foodchem.2022.133906.

Scossa, F., Benina, M., Alseekh, S., et al., 2018. The integration of metabolomics and nextgeneration sequencing data to elucidate the pathways of natural product metabolism in medicinal plants. Planta Med. 84, 855–873. https://doi.org/10.1055/a-0630-1899.

Shao, S.Y., Zhang, F., Yang, Y.N., et al., 2021. Neuroprotective and anti-inflammatory phenylethanoid glycosides from the fruits of Forsythia suspensa. Bioorg. Chem. 113, 105025 https://doi.org/10.1016/j.bioorg.2021.105025.

Tsugawa, H., Rai, A., Saito, K., et al., 2021. Metabolomics and complementary techniques to investigate the plant phytochemical cosmos. Nat. Prod. Rep. 38, 1729–1759. https://doi.org/10.1039/d1np00014d.

Wang, Z.Y., Xia, Q., Liu, X., et al., 2018. Phytochemistry, pharmacology, quality control and future research of Forsythia suspensa (thunb.) vahl: a review. J Ethnopharmacol. 210, 318–339. https://doi.org/10.1016/j.jep.2017.08.040.

Wörheide, M.A., Krumsiek, J., Kastenmüller, G., et al., 2021. Multi-omics integration in biomedical research - a metabolomics-centric review. Anal. Chim. Acta. 1141, 144–162. https://doi.org/10.1016/j.aca.2020.10.038.

Yang, F., Zou, Y.F., Li, C.Y., et al., 2022. Discovery of potential hypoglycemic metabolites in cassiae semen by coupling UHPLC-QTOF-MS/MS combined plant metabolomics and spectrum-effect relationship analyses. Food Funct. 13 (19), 10291–10304. https://doi.org/10.1039/d2fo00562j.

Zeng, S.L., Li, S.Z., Lai, C.J.S., et al., 2018. Evaluation of anti-lipase activity and bioactive flavonoids in the citri reticulatae Pericarpium from different harvest time. Phytomedicine 43, 103–109. https://doi.org/10.1016/j.phymed.2018.04.008.

Zhang, Y.Y., Feng, F., Chen, T., et al., 2016. Antidiabetic and antihyperlipidemic activities of Forsythia suspensa (thunb.) vahl (fruit) in streptozotocin-induced diabetes mice. J. Ethnopharmacol. 192, 256–263. https://doi.org/10.1016/j.jep.2016.07.002.

Zhang, F.X., Li, Z.T., Li, C., et al., 2020. Characterization of lignans in forsythiae fructus and their metabolites in rats by ultra-performance liquid chromatography coupled time-of-flight mass spectrometry. J. Pharm Pharmacol. 72, 1879–1892. https://doi.org/10.1111/jphp.13346.

Zhang, J., Li, L., Wang, J., et al., 2023. A strategy for antioxidant quality evaluation of Aster yunnanensis based on fingerprint-activity relationship modeling and chemometric analysis. Arab. J. Chem. 16, 104755 https://doi.org/10.1016/j.arabjc.2023.104755.

Zhang, L.L., Saber, F.R., Rocchetti, G., et al., 2021. UHPLC-QTOF-MS based metabolomics and biological activities of different parts of Eriobotrya japonica. Food Res. Int. 143, 110242 https://doi.org/10.1016/j.foodres.2021.110242.

Zhou, M.Y., Huo, J.H., Wang, C.R., et al., 2022. UPLC/Q-TOF MS screening and identification of antibacterial compounds in Forsythia suspensa (thunb.) vahl leaves. Front. Pharmacol. 12, 704260 https://doi.org/10.3389/fphar.2021.704260.